An iterative method to infer distributed mass and stiffness profiles for use in reference dynamic beam-Winkler models of foundation piles from frequency response functions

Wu, W. H.; Prendergast, L. J.; Gavin, K.

DOI
10.1016/j.jsv.2018.05.049

Publication date
2018

Document Version
Final published version

Published in
Journal of Sound and Vibration

Citation (APA)
Wu, W. H., Prendergast, L. J., & Gavin, K. (2018). An iterative method to infer distributed mass and stiffness profiles for use in reference dynamic beam-Winkler models of foundation piles from frequency response functions. *Journal of Sound and Vibration*, *431*, 1-19. https://doi.org/10.1016/j.jsv.2018.05.049

Journal of Sound and Vibration 431 (2018) 1–19

Contents lists available at ScienceDirect

Journal of Sound and Vibration

journal homepage: www.elsevier.com/locate/jsvi

An iterative method to infer distributed mass and stiffness profiles for use in reference dynamic beam-Winkler models of foundation piles from frequency response functions

W.H. Wu [a], L.J. Prendergast [b,*], K. Gavin [b]

[a] Department of Construction Engineering, National Yunlin University of Science and Technology, No. 123, Section 3, University Road, Douliu City, Yunlin 640, Taiwan

[b] Faculty of Civil Engineering and Geosciences, Delft University of Technology, Building 23, Stevinweg 1, PO-box 5048, 2628 CN Delft, 2600 GA Delft, The Netherlands

ARTICLE INFO

Article history:
Received 16 October 2017
Received in revised form 14 May 2018
Accepted 31 May 2018
Available online 6 June 2018
Handling Editor: I. Trendafilova

Keywords:
Soil stiffness
Model-updating
Dynamics
Mass
Winkler
SSI

ABSTRACT

Accurate characterisation of soil behaviour in Dynamic-Soil-Structure Interaction (DSSI) applications remains a significant challenge. Knowledge of the operational soil-structure interaction stiffness is important for applications ranging from earthquake engineering to offshore structures subjected to wind and wave loading. A number of methods have been derived to couple soil and structural properties using beam-Winkler models. One of the key drawbacks of these approaches is the disparity in predicted stiffness depending on the formulation chosen. Moreover, the contribution of soil mass in the dynamic motion of foundations is often neglected. In this paper, a method is presented that uses a Frequency Response Function (FRF) measured from a laterally-impacted pile to estimate operational stiffness and mass profiles acting along the pile. The method involves creating a beam-Winkler numerical model of the soil-pile system, applying a starting estimate of the soil stiffness and mass profiles and calculating weighting factors to be applied to these starting estimates to obtain a match between the measured FRF from the test pile and the calculated FRF from the numerical model. This paper presents the formulation of the iterative updating approach, and demonstrates its functionality using simulated experimental data of typical piles. Simulated data is used as it enables testing a wide range of circumstances including possible issues relating to the influence of the shape of the operational soil stiffness profile, soil density, effects of sensor noise and errors in damping estimation. The method may be useful in finite-element (FE) model updating applications where reference numerical models for soil-structure interaction are required.

1. Introduction

The dynamic response of soil-structure interaction (DSSI) systems is an area of growing research interest. It is a topic with applications in Earthquake Engineering [1,2], Offshore Engineering [3,4] and Structural Health Monitoring (SHM) [5–8], among others. The offshore wind energy sector is undergoing a phase of rapid expansion [9,10], with monopile foundations

* Corresponding author.
E-mail addresses: wuwh@yuntech.edu.tw (W.H. Wu), l.j.prendergast@tudelft.nl (L.J. Prendergast), k.g.gavin@tudelft.nl (K. Gavin).

https://doi.org/10.1016/j.jsv.2018.05.049
0022-460X/

tending towards larger diameters, a phenomenon that is adding growing uncertainty regarding dynamic stability and lifespan of these systems and calling into question existing design approaches. The issue is complex as the dynamic response of soil is strongly dependent on the particle size, geological history, age of the deposit, degree of cementation and the nonlinear stress-strain behaviour among many other factors. Moreover, soil-structure interaction responses are heavily influenced by the nature of loading applied and are affected by load magnitude, rate of application, frequency of loading, stress-history, pore pressure accumulation and dissipation among other factors. In concert with this, there is increasing agreement that design procedures which were originally derived for flexible piles [11,12] may not offer a reasonable estimate of the operating soil-structure interaction stiffness in these stiffer systems [13].

In the field of vibration-based SHM, the dynamic response of a structure is used to infer the presence of damage, such as cracking or corrosion [14,15]. More recently, several authors have begun to look at detecting foundation damage, such as scour erosion, using the vibration-response of a structure [5–7,16,17]. Many of these methods rely on the creation of a reference numerical model of the system [5,8,18–20], for which accurate DSSI stiffness is paramount to obtain matches to experimental data [21]. Recent studies [22,23] have shown that the adoption of a variety of existing models to couple soil and structural properties in a beam-Winkler framework leads to a significant disparity in predicted responses. If reference DSSI models cannot obtain good matches under normal operation, damage effects cannot easily be separated from otherwise normal operating behaviour.

In addition to differences in the various models used to characterise SSI coupling stiffness, the inherently variable nature of soil means accurate characterisation of its properties is challenging. Predicted dynamic responses from numerical models incorporating soil stiffness will be heavily dependent on the accuracy of the soil response characteristics. Reducing the uncertainty will require either (i) a concerted effort to develop new testing practices that reduce or mitigate the errors and unknowns and/or, (ii) the development of suitable model updating approaches to evaluate operating soil characteristics (mass, damping and stiffness) based on simple experimental techniques. The focus of this paper is on the latter, so more attention is given over to existing methods developed herein.

Updating of numerical models using experimental data has received significant attention in the literature [24–32]. Imregun et al. [24] present a FRF-based FE updating method. Using a simple beam model and both simulated and real experimental data, they investigate several performance parameters such as the uniqueness of the updated model, performance against noisy and incomplete data and the effect of excitation direction, among others. They conclude that uniqueness of the solution remains an issue and that noise has a deleterious effect on the error location. Nalitolela et al. [25] present a method for updating model parameters by hypothesising the addition of an imagined stiffness to the structure. FRF data for the structure with imagined stiffness is obtained from the measured FRF of the actual structure. Using eigenvalues derived from the FRFs and from an analytical model of the system, the structural parameters are updated by a sensitivity procedure. The method is demonstrated using simulated and experimental data. Mottershead et al. [26] present a tutorial on the use of the sensitivity method in FE updating. The sensitivity method is based on linearization of the generally nonlinear relationship of measurement outputs (frequencies, mode shapes, displacements etc.) and the model parameters in need of adjustment. A large scale helicopter airframe model updating example is used to demonstrate the procedure. Esfandiari et al. [28] present a FRF-based method to update structural mass and stiffness using vibration data, for the purpose of damage identification. The procedure is demonstrated using a numerical truss model, with simulated noise presence. The method successfully identified location and severity of damage in stiffness and mass when high excitation frequencies are applied. Similarly, Hwang and Kim [27] present a FRF-based method to estimate the location and severity of damage in a structure, and present numerical examples of a simple cantilever and helicopter rotor blade.

Many of the updating procedures described previously are based on FRF data [24,27,28,30,31] and most are demonstrated with application to simple structural examples such as beams or trusses. A method capable of application to pile foundations, which can obtain a reasonable estimate of the operating soil stiffness and mass acting in the dynamic motion, is therefore of interest. In this paper, a method that establishes operational soil stiffness and mass profiles contributing to the dynamic behaviour of a pile in a soil-structure interaction problem is presented, using a FRF-based updating approach. The approach requires a single measured FRF from a target pile and the creation of a reference beam-Winkler model, with an initial guess of the operational soil stiffness and mass. The initial stiffness guess should be informed from geotechnical data, which broadly captures the distribution of stiffness with depth. The method minimises the difference in peak information between target and calculated FRF data of acceleration by updating the guess for the initial stiffness and mass by multiplying these by weightings. An iterative solution is postulated, as due to the distributed mass and stiffness properties of beam-Winkler models (piles), separately updating mass and stiffness is not possible. The developed approach is demonstrated using numerically generated pile FRF data and a range of conditions are trialled, including various pile geometries and distributions of soil stiffness. The effect of noise intrusion (in 'sensors') and measurement error in damping are also investigated. The goal of this study is to postulate an approach that can successfully estimate the stiffness and mass acting on a pile with a view to informing a reference damage model or to enable more insight into operating parameters for improved design procedures. For DSSI applications, inferring distributed mass and stiffness using a single FRF (force-acceleration pair) is reasonable due to the relatively crude approximations required for these applications in reality. Section 2 presents the theoretical background behind the modelling methods employed and information on the target pile models developed to test the procedure, Section 3 presents details of the iterative procedure developed for updating soil stiffness and mass using FRFs, Section 4 presents the results of the analysis, and Section 5 describes how to apply the procedure to real piles.

2. Numerical modelling

In Section 2.1, the methods employed to numerically model a Finite-Element (FE) dynamic beam-Winkler system used in the present study, and from which to obtain FRF information are discussed. The subsequent Section 2.2 presents information on the development of target numerical (pile) models used in this paper to test the iterative procedure.

2.1. Numerical modelling of beam-Winkler system

A FE model of a beam-Winkler system (numerical analogue of a pile embedded in soil) is programmed in MATLAB. This model is used as a reference numerical model to obtain FRF information for the iterative procedure described in Section 3. Euler-Bernoulli beam elements are used to model a pile, the consistent mass and stiffness matrices for which are available in Ref. [33]. The soil is modelled using discrete, closely-spaced and mutually independent Winkler spring elements [19,22,34,35], see schematic shown in Fig. 1(b). Point masses lumped at the pile nodes attached to each Winkler spring allow the incorporation of soil mass. A global equation of motion for the MDOF dynamic system can be formulated as shown in Eq. (1).

$$[\mathbf{M_G}]\begin{Bmatrix}\ddot{x}_1(t)\\ \ddot{x}_2(t)\\ \vdots\\ \ddot{x}_N(t)\end{Bmatrix}+[\mathbf{C_G}]\begin{Bmatrix}\dot{x}_1(t)\\ \dot{x}_2(t)\\ \vdots\\ \dot{x}_N(t)\end{Bmatrix}+[\mathbf{K_G}]\begin{Bmatrix}x_1(t)\\ x_2(t)\\ \vdots\\ x_N(t)\end{Bmatrix}=\begin{Bmatrix}F_1(t)\\ F_2(t)\\ \vdots\\ F_N(t)\end{Bmatrix} \tag{1a}$$

$$\text{or}\quad [\mathbf{M_G}]\{\ddot{\mathbf{x}}(t)\}+[\mathbf{C_G}]\{\dot{\mathbf{x}}(t)\}+[\mathbf{K_G}]\{\mathbf{x}(t)\}=\{\mathbf{F}(t)\} \tag{1b}$$

where $\mathbf{[M_G]}$, $\mathbf{[C_G]}$ and $\mathbf{[K_G]}$ are the $(N \times N)$ global mass, damping and stiffness matrices for the model respectively, N is the total number of degrees of freedom in the system. The vector $\{\mathbf{x}(t)\}$ describes the displacement of every degree of freedom for each time step in the analysis. Similarly the vectors $\{\dot{\mathbf{x}}(t)\}$ and $\{\ddot{\mathbf{x}}(t)\}$ describe the velocity and acceleration of every degree of freedom for each time step. The vector $\{\mathbf{F}(t)\}$ describes the external forces acting on each of the degrees of freedom at a given time step in the numerical model.

The damping matrix $\mathbf{[C_G]}$ is formulated using a two-term Rayleigh damping formulation [36], as a linear combination of $\mathbf{[M_G]}$ and $\mathbf{[K_G]}$. It is formulated as follows in Eqs. (2) and (3).

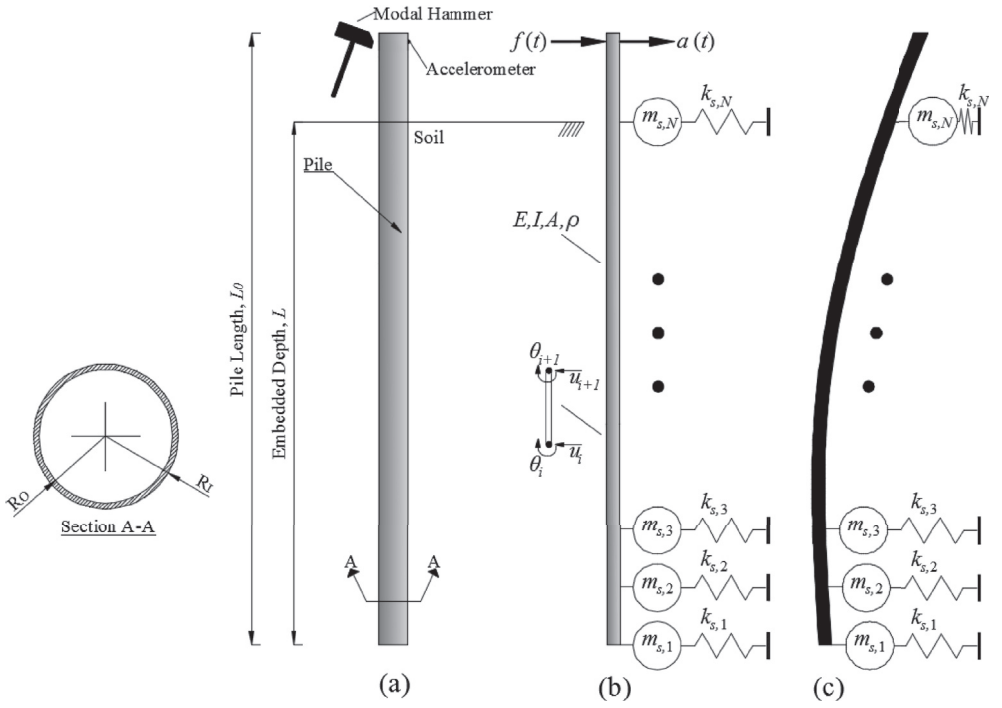

Fig. 1. Model schematic, (a) pile geometry, (b) numerical schematic of beam-Winkler system, (c) first mode shape schematic.

$$\begin{Bmatrix} \xi_1 \\ \xi_2 \end{Bmatrix} = \frac{1}{2}\begin{bmatrix} \frac{1}{\omega_1} & \omega_1 \\ \frac{1}{\omega_2} & \omega_2 \end{bmatrix}\begin{Bmatrix} \alpha_0 \\ \alpha_1 \end{Bmatrix} \Rightarrow \begin{Bmatrix} \alpha_0 \\ \alpha_1 \end{Bmatrix} = \frac{2\omega_1\omega_2}{\omega_2^2-\omega_1^2}\begin{bmatrix} \omega_2 & -\omega_1 \\ -\frac{1}{\omega_2} & \frac{1}{\omega_1} \end{bmatrix}\begin{Bmatrix} \xi_1 \\ \xi_2 \end{Bmatrix} \tag{2}$$

where ξ_1 and ξ_2 are the modal damping ratios for the first and second vibration modes respectively, ω_1 and ω_2 are the first and second circular frequencies and α_0 and α_1 are the proportionality constants for mass and stiffness respectively. The damping matrix $\mathbf{[C_G]}$ is formulated in Eq. (3).

$$[\mathbf{C_G}] = \alpha_0[\mathbf{M_G}] + \alpha_1[\mathbf{K_G}] \tag{3}$$

The time-domain dynamic response can be obtained by solving Eq. (1) using numerical integration. In this paper, the Wilson-θ integration scheme is employed, which is a special case of the linear acceleration method [37,38].

In addition to obtaining the time-domain response for the purpose of generating FRFs, the undamped natural frequencies of the system can be obtained by solving the Eigenproblem [37]. These undamped frequencies are used in the procedure of automating the FRF peak picking technique later, to allow the model perform many iterations automatically. In effect, the undamped frequency as calculated by solving the Eigenproblem is used to localise the peak corresponding to the first natural frequency in the generated FRF, to ensure the correct peak is identified (using a simplified max peak approach may choose a different mode).

A general schematic of the model used in this paper is shown in Fig. 1. Fig. 1(a) shows a schematic of the pile geometry. A given pile is created by specifying the fundamental geometrical information (diameter, wall thickness, length and embedded depth). A numerical schematic is shown in Fig. 1(b), created by discretising the pile into finite-elements, each of length 0.1 m. The embedded portion of the pile has Winkler springs attached, spaced at 0.1 m centres. In each case, point masses are applied to the top quarter of springs in each model, with the lower masses set to zero. This is undertaken as a means to remain physically in keeping with the expected motion of a real pile, which will be dominated by the first mode of vibration, and as such will exhibit more movement near the ground surface than at depth [22], see Fig. 1(c). Applying masses at lower elevations will therefore have limited effect on the first mode shape, and so are omitted. An impulse force vector is applied to the lateral DOF at the pile head $f(t)$, and the resulting acceleration $a(t)$ is calculated at the same location, by solving the matrix differential Eq. (1). This information is then used to create FRFs.

2.2. Development of target benchmark models

The method to identify operational soil stiffness and mass profiles from frequency response functions is demonstrated numerically using simulated target FRF data, obtained through the modelling of impact testing of reference numerical models of piles. The reference pile models are programmed using the procedure from the previous Section 2.1, and have varied geometrical parameters (diameters, lengths), soil stiffnesses and masses. In order to make the FRFs as realistic as possible, the effect of sensor noise is investigated, as the signals from real piles subjected to impact testing contain certain noise intrusion [3,21,22,39,40]. The reference numerical models represent piles that have been impact tested, using a modal hammer, and this information is used as the target in the iteration procedure described in Section 3.2. The assumptions and methods are outlined herein, for a given reference pile.

A total of 34 target pile models are simulated and FRFs are obtained by simulating an impact test applied laterally to the pile head in each model. Each model has a certain diameter, D, annular thickness, $t_0 = 0.025$ m, embedded length, L, and length, $L_0 = L+1$ m. All models have a diameter, $D = 1$ m except models Target 17–20 which have $D = 4$ m. All models have the same embedment $L = 20$ m ($L_0 = 21$ m) except models Target 21–24 which have $L = 10$ m and $L_0 = 11$ m respectively. The impulse force in each case is taken as 10,000 N applied for a period of 0.015 s, to represent the act of impacting a pile with a modal hammer (see Fig. 1). Table 1 outlines the remaining parameters used in each of the 34 target models that vary from these properties. A damping ratio of $\xi_1 = 3\%$ applied to the first vibration mode and $\xi_2 = 50\%$ applied to the second mode is incorporated in each model, using the two-term Rayleigh method [36], as described in Subsection 2.1. The 3% damping ratio for mode 1 was adopted to reasonably estimate energy dissipation from fully embedded piles. This value is higher than that measured in Prendergast and Gavin [22], who measured damping ratios of 1.8% and 1.26% for two piles with embedded lengths of 4.5 m and 3.1 m and free (above ground) lengths of 2.5 m and 3.9 m respectively. As the simulated piles in this paper are close to fully embedded, the higher damping ratio is adopted. The 50% damping for mode 2 is to suppress the influence of higher vibration modes because in the real case, the dynamic response of a pile to an impact load at the head will be dominated by the first natural frequency with little contribution from higher modes [22]. A more complicated model would be required to accurately encapsulate the numerous damping effects at play in real soil-pile interaction such as radiation and hysteretic damping, therefore the simplification adopted to suppress higher modes is based on experimental observations from previous pile vibration tests [22].

In order to ensure the target models adequately represent piles in the real case, soil stiffness is derived using the geotechnical procedure outlined herein. On a real pile, soil stiffness can be estimated from shear wave velocity measurements, or from correlations to Cone Penetration Tests (CPT), among other methods [13,21,22,41,42]. So, for the present

Table 1
Benchmark model parameters.

Name	Soil Profile	Soil Density	Target w_m	Target w_k	SNR
Target 1	Constant	Loose	5	0.75	–
Target 2	Constant	Loose	5	0.85	–
Target 3	Constant	Loose	5	1.15	–
Target 4	Constant	Loose	5	1.25	–
Target 5	Constant	Loose	10	0.75	–
Target 6	Constant	Loose	10	0.85	–
Target 7	Constant	Loose	10	1.15	–
Target 8	Constant	Loose	10	1.25	–
Target 9	Parabolic	Loose	5	0.75	–
Target 10	Parabolic	Loose	5	0.85	–
Target 11	Parabolic	Loose	5	1.15	–
Target 12	Parabolic	Loose	5	1.25	–
Target 13	Parabolic	Loose	10	0.75	–
Target 14	Parabolic	Loose	10	0.85	–
Target 15	Parabolic	Loose	10	1.15	–
Target 16	Parabolic	Loose	10	1.25	–
Target 17	Constant	Loose	5	0.75	–
Target 18	Constant	Loose	10	1.25	–
Target 19	Parabolic	Loose	5	0.75	–
Target 20	Parabolic	Loose	10	1.25	–
Target 21	Constant	Loose	5	0.75	–
Target 22	Constant	Loose	10	1.25	–
Target 23	Parabolic	Loose	5	0.75	–
Target 24	Parabolic	Loose	10	1.25	–
Target 25	Constant	Dense	5	0.75	–
Target 26	Constant	Dense	10	1.25	–
Target 27	Parabolic	Dense	5	0.75	–
Target 28	Parabolic	Dense	10	1.25	–
Target 29	Constant	Loose	5	0.75	20
Target 30	Constant	Loose	10	1.25	20
Target 31	Constant	Loose	5	0.75	10
Target 32	Constant	Loose	10	1.25	10
Target 33	Constant	Loose	5	0.75	5
Target 34	Constant	Loose	10	1.25	5

purpose, idealised soil profiles corresponding to two soil densities are created. It is assumed that the profiles hypothesised herein could be estimated from actual site investigative data. Two types of soil profile shape are tested in this paper, (i) a constant stiffness profile with uniform stiffness over the pile depth, and (ii) a parabolic stiffness profile, where the soil stiffness increases nonlinearly with mean stress level. Fig. 2 shows an example of both profile types, for idealised loose sand. For the constant soil profile, shear moduli (G) of 25 MPa and 75 MPa are specified to represent loose and dense sand profiles respectively [22], to cover the range of expected densities. Shear moduli can be converted to profiles of the modulus of subgrade reaction, K (soil-structure coupling stiffness), using the procedure outlined in Refs. [21,22,43], and to individual Winkler spring constants by multiplying by the spacing between each Winkler spring in the model (0.1 m). For the parabolic soil profile, a second method is used to specify a soil profile via the generation of idealised CPT q_c profiles, which can be correlated directly to soil springs [3]. Sand is classified into relative density, D_r categories of 30% (loose sand) and 80% (dense sand) [44]. An expression postulated by Lunne and Christopherson [45] is re-arranged to relate this D_r to a CPT q_c tip resistance, as shown in Eq. (4) [3].

$$q_c = 60\left(\sigma'_v\right)^{0.7} e^{2.91 D_r} \tag{4}$$

where σ'_v is the vertical effective stress (kN m^{-2}). The q_c profile can then be converted to a shear modulus profile using the rigidity index, $G = nq_c$ a correlation developed for a range of conditions by Lunne et al. [46] and Schnaid et al. [47]. When age, degree of cementation and stress history are considered, these parameters can be reasonably well estimated. The derived shear modulus profile using this method is converted to the modulus of subgrade reaction, K using the same method as previously described, then to individual spring moduli, $k_{s,i}$.

The procedure for generating target FRF information is as follows. An impulse force $f(t)$ is modelled, and is inputted into the numerical model for a given reference pile. The acceleration of the system is calculated by solving the dynamic equation of motion, Eq. (1) using numerical integration (Wilson-theta technique [38]). The input force time-history and the output acceleration response are used to derive the remaining required information. A FRF for the acceleration can be directly calculated by taking the ratio for the Fourier transform of the generated output acceleration to that of the generated input force. On a real pile, the acceleration would be measured using an accelerometer and the velocity and displacement are typically not measured. To represent this assumption in the reference (target) models, the corresponding FRFs for velocity and

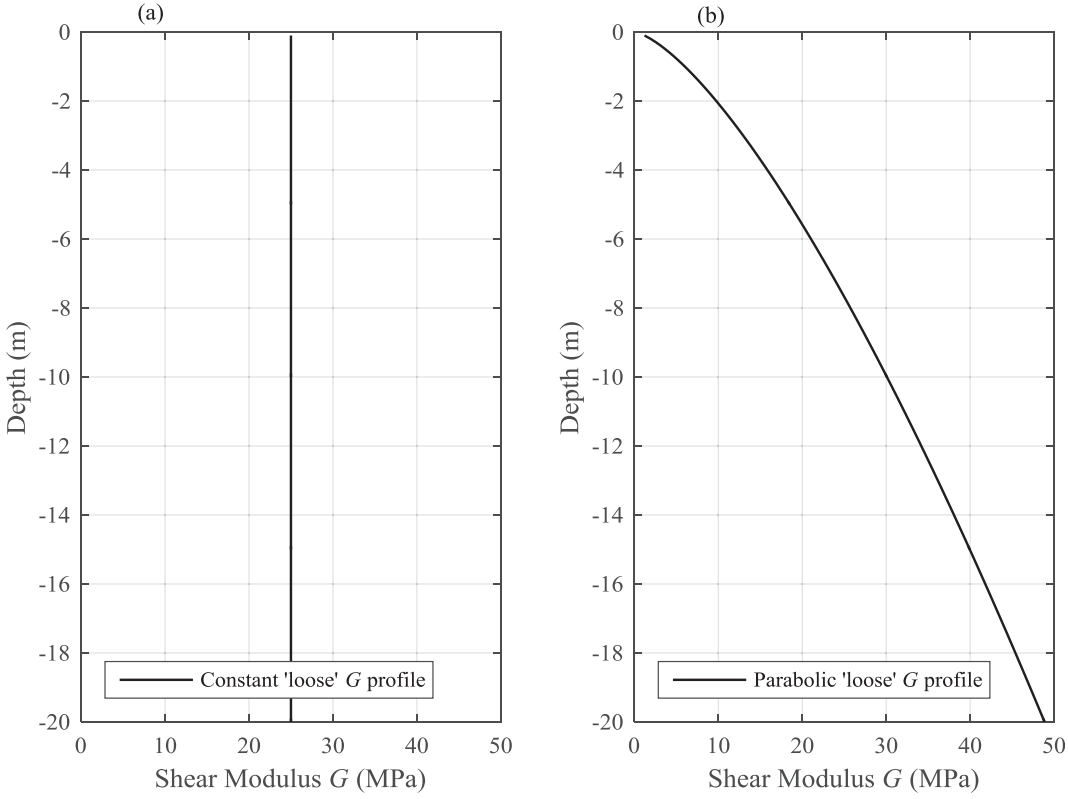

Fig. 2. Soil profile types used in analysis, (a) constant stiffness profile, (b) parabolic stiffness profile.

displacement are derived directly from the acceleration FRF by the relationships expressed in Eqs. (7) and (8) respectively, as opposed to calculating them by solving Eq. (1). Note, this assumption introduces minor errors to the analysis, but is in keeping with the reality of the physical system.

Target models 29 to 34 contain added measurement noise. The procedure for adding noise is based on the Signal-to-Noise Ratio (SNR), as described in Lyons [48]. The addition of noise is to replicate the conditions of a real pile, whereby the sensors would experience some interference [39]. Moderate (SNR = 20) to severe (SNR = 5) noise levels are added in these models and the method is tested in Section 4.4.

Table 1 shows the details of each target model and a brief description of how each is developed is provided herein. A model is developed containing certain geometrical information and a profile of stiffness and mass is specified. The stiffness and mass profiles are then altered by multiplying by specified weightings, and these weightings are used to appraise the performance of the FRF-based updating method described later. These weightings are defined as (i) w_m, the mass weighting which multiplies the pile mass and distributes it as additional mass to the sprung pile nodes and, (ii) w_k, the stiffness weighting which multiplies the postulated soil stiffness profile. For example, Target 1 has a constant soil profile of 'loose' sand ($G = 25$ MPa). The soil stiffness is multiplied by the target weighting, $w_k = 0.75$, to reduce the 'acting' stiffness. A soil mass of 5 times the pile mass ($w_m = 5$) is distributed to the pile nodes where the top quarter of springs are located in the model, as point masses (see Fig. 1(b)). Target 1 is then stored as a FRF of acceleration, due to the applied impulse force, and used as the target to test the model updating approach. If the model updating method converges on the same mass and stiffness weightings, it is successful.

3. Iterative solution procedure to infer mass and stiffness from FRFs

In this section, the iterative procedure to infer soil mass and stiffness is presented. It is first necessary to provide a brief overview of the derivation of FRFs for single-degree-of-freedom systems with discussion as to their applicability to multi-degree-of-freedom (MDOF) systems in the present context, as this is key to the iterative method subsequently presented. Section 3.2 provides details of the iterative method used to converge on operational stiffness and mass in dynamic beam-Winkler models.

3.1. Frequency response functions

The equation of motion for a single-degree-of-freedom (SDOF) system (or a particular mode of a MDOF system) in the time-domain is represented by Eq. (5).

$$m\ddot{x}(t) + c\dot{x}(t) + kx(t) = f(t) \tag{5a}$$

$$\text{or} \quad \ddot{x}(t) + 2\xi\omega\dot{x}(t) + \omega^2 x(t) = f(t)/m \tag{5b}$$

where m is the mass, k is the stiffness, c is the damping, $f(t)$ is the excitation force applied, $x(t)$ is the dynamic displacement, $\dot{x}(t)$ is the velocity, $\ddot{x}(t)$ is the acceleration, $\omega \equiv \sqrt{k/m}$ and the damping ratio, $\xi \equiv c/(2m\omega)$. Eq. (5) can be transformed into the frequency domain by developing a FRF as shown in Eq. (6).

$$H_d(\overline{\omega}) = \frac{X(\overline{\omega})}{F(\overline{\omega})} = \frac{1}{m\left(-\overline{\omega}^2 + 2i\xi\omega\overline{\omega} + \omega^2\right)} = \frac{1}{m\omega^2\left[\left(1-\beta^2\right) + 2i\xi\beta\right]} = \frac{1}{k\left[\left(1-\beta^2\right) + 2i\xi\beta\right]} \tag{6}$$

where $\overline{\omega}$ is the variable of excitation, $X(\overline{\omega})$ and $F(\overline{\omega})$ are the Fourier transforms of $x(t)$ and $f(t)$ respectively and $\beta \equiv \overline{\omega}/\omega$. Eq. (6) is the FRF of the displacement response of the SDOF system to the excitation force. Similarly, one can deduce the velocity response to the excitation force in Eq. (7) and the acceleration response to the excitation force in Eq. (8).

$$H_v(\overline{\omega}) = i\overline{\omega}H_d(\overline{\omega}) = \frac{i\overline{\omega}}{m\omega^2\left[\left(1-\beta^2\right) + 2i\xi\beta\right]} = \frac{i\beta}{m\omega\left[\left(1-\beta^2\right) + 2i\xi\beta\right]} = \frac{i\beta}{\sqrt{km}\left[\left(1-\beta^2\right) + 2i\xi\beta\right]} \tag{7}$$

$$H_a(\overline{\omega}) = -\overline{\omega}^2 H_d(\overline{\omega}) = \frac{-\overline{\omega}^2}{m\omega^2\left[\left(1-\beta^2\right) + 2i\xi\beta\right]} = \frac{-\beta^2}{m\left[\left(1-\beta^2\right) + 2i\xi\beta\right]} \tag{8}$$

The amplitudes of the FRFs in Eqs. (6)–(8) are described by Eqs. (9)–(11) for displacement ($F_d(\overline{\omega})$), velocity ($F_v(\overline{\omega})$) and acceleration ($F_a(\overline{\omega})$) respectively.

$$F_d(\overline{\omega}) \equiv |H_d(\overline{\omega})| = \frac{1}{k\sqrt{\left(1-\beta^2\right)^2 + 4\xi^2\beta^2}} \tag{9}$$

$$F_v(\overline{\omega}) \equiv |H_v(\overline{\omega})| = \frac{\beta}{\sqrt{km\left[\left(1-\beta^2\right)^2 + 4\xi^2\beta^2\right]}} \tag{10}$$

$$F_a(\overline{\omega}) \equiv |H_a(\overline{\omega})| = \frac{\beta^2}{m\sqrt{\left(1-\beta^2\right)^2 + 4\xi^2\beta^2}} \tag{11}$$

With given k, m, and ξ, the maximum amplitude (peak) of each FRF can be analytically solved in Eqs. (12)–(14), for displacement, velocity and acceleration respectively.

$$(F_d)_{\max} = \frac{1}{2k\xi\sqrt{1-\xi^2}} \approx \frac{1}{2k\xi} \text{ at } \beta = \sqrt{1-2\xi^2} \approx 1 \tag{12}$$

$$(F_v)_{\max} = \frac{1}{2\sqrt{km\xi}} \text{ at } \beta = 1 \tag{13}$$

$$(F_a)_{\max} = \frac{1}{2m\xi\sqrt{1-\xi^2}} \approx \frac{1}{2m\xi} \text{ at } \beta = \frac{1}{\sqrt{1-2\xi^2}} \approx 1 \tag{14}$$

Observing Eq. (12), it is possible to know if the stiffness, k of a SDOF system is over or underestimated when compared with benchmark (target) FRF data with the same damping ratio. If the system has a peak FRF lower than that of target data, it has a higher stiffness and vice versa. Moreover, this equation should also inform if the effective k of the fundamental mode of a MDOF system with matching damping is over or underestimated. Similarly, Eq. (14) can indicate under or overestimation of the effective mass contribution, m to the fundamental mode of a MDOF system, based on the peak values. In this paper, the system under discussion is a dynamic beam-Winkler system, representative of a pile foundation embedded in a soil matrix.

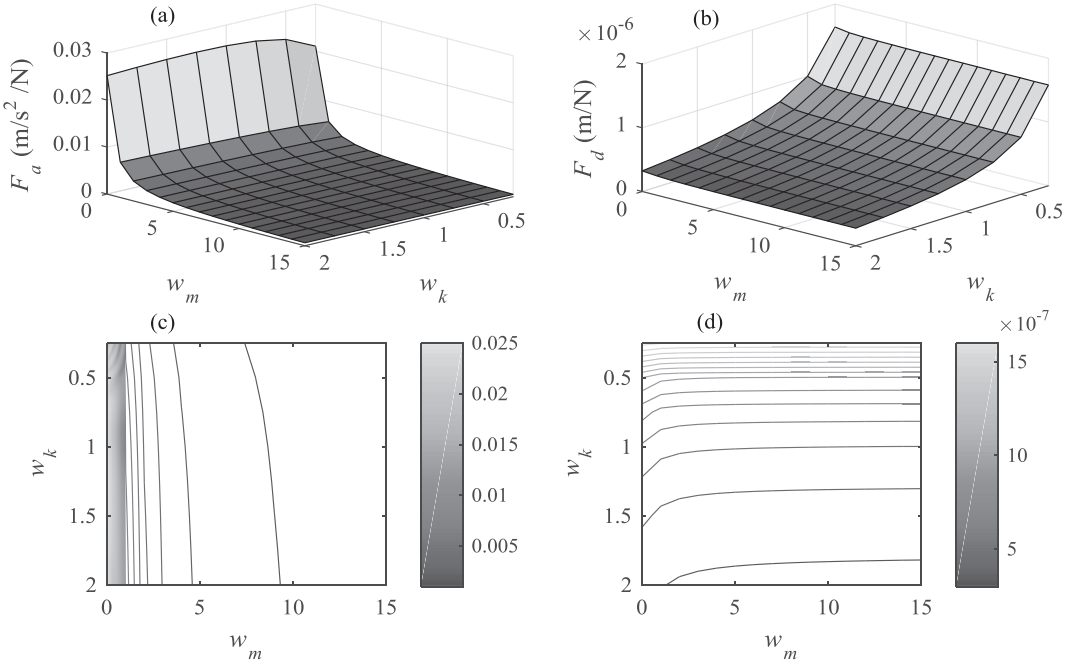

Fig. 3. Relationship between FRF peak height and mass and stiffness weightings for Target 1 model geometry ($L = 21$ m, $D = 1$ m), (a) variation of F_a with w_m and w_k, (b) variation of F_d with w_m and w_k, (c) contour plot of F_a with w_m and w_k, (d) contour plot of F_d with w_m and w_k.

This type of system has distributed mass and stiffness properties (see Fig. 1), therefore its behaviour will deviate from that of a SDOF system. This means it is not possible to directly infer the stiffness or mass contribution using the SDOF derivations previously for F_a and F_d. Instead, by developing an effective iterative algorithm, it is possible to use the information presented in this section to converge on operational stiffness (w_k) and mass (w_m) weightings applied to estimated profiles in the dynamic modelling of a particular pile-soil problem. To illustrate this concept for a MDOF system, an analysis is conducted herein where the variation in peak FRF F_a and F_d for a pile model with respect to variations in soil mass and stiffness acting in the dynamic model is extracted. Fig. 3 shows the results for the pile model Target 1 (see Table 1), which is 21 m in length and has a diameter of 1 m and Fig. 4 shows the same analysis but for the stiffer pile model Target 17 ($L = 21$ m, $D = 4$ m). Both analyses are conducted with Rayleigh damping, where a damping ratio ($\xi_1 = \xi_2 = \xi$) of 1% is specified. This system is dominated by several vibration modes, therefore the results should vary from a SDOF model (in that the FRF peaks for acceleration and displacement should be affected by both changes in mass and stiffness, and not simply by changes in these parameters individually). Fig. 3(a) shows how the acceleration FRF F_a varies with mass and stiffness weighting and Fig. 3(b) shows how the displacement FRF F_d varies with these weightings. Fig. 3(c) and (d) show contour plots for F_a and F_d respectively. F_a varies predominately with the changes in mass weighting with minor variations due to changes in stiffness weighting. F_d varies predominately with stiffness weighting with minor variations due to mass weighting. This analysis implies that a unique set of weightings can be used to characterise a given set of circumstances, i.e. a given pair of weightings $\{w_m, w_k\}$ gives rise to a unique model for pile stiffness and mass. Section 3.2 presents the FRF-based updating method founded on this premise.

3.2. Mass and stiffness iteration algorithm

In this section, the basis of an iterative solution method to establish the operating stiffness and mass from FRF data in a MDOF dynamic beam-Winkler model is presented. The simulated experimental data is referred to as 'target' data (see Table 1). The calculated FRF within the iteration scheme is referred to as 'calculated' data. Observing Eq. (14), for a SDOF system, the mass, m in a model can be modified according to the ratio of the peak values of FRF amplitude F_a in the target and calculated signals. The stiffness, k can then be adjusted according to the ratio of the peak target and calculated frequencies or the ratio of the peak values of FRF amplitude F_d (Eq. (12)) depending on numerical accuracy. For a beam-Winker MDOF model, the nature of distributed masses and spring stiffnesses means an iteration-based algorithm is called for, as this type of system will deviate in behaviour somewhat from a SDOF simple system (see Fig. 3 for the variation of each peak, F_a and F_d, with both mass and stiffness weighting). However, broadly speaking the F_a ratios mainly provide insight into the mass contribution and the F_d ratios or frequency ratios provide insight into the operating stiffness, though some cross-coupling occurs between these mechanisms for distributed systems (see Fig. 3). By postulating a linear mechanical system (small-strain criterion for Winkler springs), an algorithm is developed using linear projection, which requires two initial starting points.

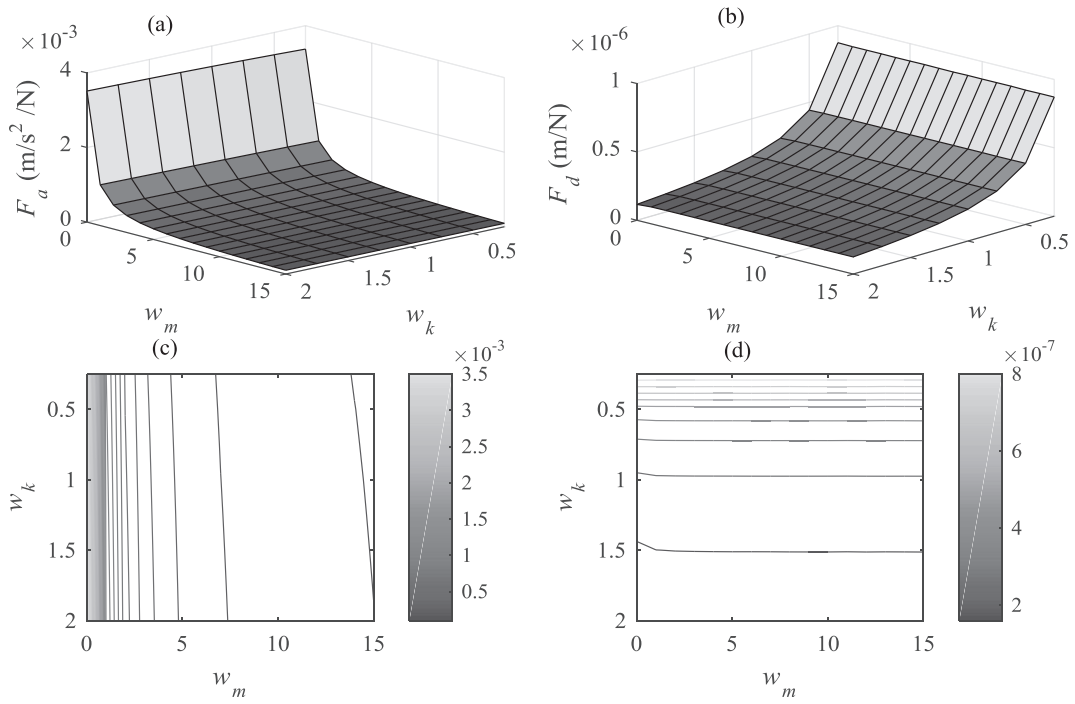

Fig. 4. Relationship between FRF peak height and mass and stiffness weightings for Target 17 model geometry ($L = 21$ m, $D = 4$ m), (a) variation of F_a with w_m and w_k, (b) variation of F_d with w_m and w_k, (c) contour plot of F_a with w_m and w_k, (d) contour plot of F_d with w_m and w_k.

Define $r_m = F_{a,\text{TARGET}}/F_{a,\text{CALCULATED}}$ (ratio of target to numerically calculated peak heights in acceleration FRF) and $r_\omega = f_{\text{CALCULATED}}/f_{\text{TARGET}}$ (ratio of calculated frequency to target frequency), see Fig. 5. Let m_p = mass of the full beam-Winkler system (pile) and n = number of beam nodes connected to a Winkler spring in the numerical model (no. of embedded nodes in a foundation pile analogue). An initial starting estimate is required, so the initial stiffness weighting is assumed as 1 times a proposed soil stiffness profile. Note, an estimate of the soil stiffness is required at the beginning of the problem, then the algorithms weight this profile to obtain convergence. Soil-structure interaction stiffness for real systems can be estimated from geotechnical site investigative data such as Cone Penetration Test data [3,13,21,49,50] or shear wave velocity measurements [41,47,51], which are readily taken prior to construction, see Section 2.2. For the purposes of this paper, the shape of the soil stiffness profiles are assumed to be known beforehand, but the actual operating magnitudes at each depth are assumed to be incorrect (so that the algorithm can converge on correct profile weightings). The assumption of knowing the broad trend and approximate magnitude of the operating soil stiffness is in keeping with reality, as for an offshore pile design, an estimate of soil stiffness is obtainable using geotechnical testing methods, so it is assumed the same information would be available for the purpose of the numerical study undertaken in this paper. Define two convergence criteria, ε_ω is the frequency convergence tolerance and ε_m is mass convergence tolerance. Both of these are assumed as 1%. The algorithm is outlined in the flow chart in Fig. 6.

Target acceleration FRF data is obtained from a 'test' pile – i.e. the target models in Table 1. The geometries of this test system are known to the user, so a reference numerical model is built using the same geometrical and material properties. An estimated soil stiffness profile is applied in the reference model (the shape of which is assumed as known a-priori, the magnitude being incorrect). Soil mass, equating to the weighted pile mass, is equally distributed between active spring nodes. The active nodes for all analyses in this paper are taken as the top quarter springs ($n/4$) to remain in keeping with a physical pile which would be dominated by the first bending mode. An initial mass weighting is calculated as a uniformly distributed number between 0 and 30 to be multiplied by the pile mass and distributed at the active nodes. The modal hammer information used in the 'test' pile to obtain the target data, is inputted directly into the reference model to calculate the FRF from the calculated acceleration response, obtained by solving Eq. (1). The damping ratio measured from the target response is also input into the reference model, to formulate the Rayleigh damping matrix. Damping can be measured from a response using techniques such as logarithmic decrement [52] or exponential curve fitting [53], among others. The calculated FRF data and the target FRF data are used to obtain r_m, r_ω and subsequently, r_k. Depending on the magnitude of r_m, the soil mass is either increased or decreased as the initial guess either overestimates of underestimates this contribution. The second guess for the stiffness weighting is taken as a uniformly distributed random number between 0.7 and 1.3 times the postulated soil stiffness profile. Note, it is not important what value of stiffness is taken as the second guess, it is merely required that the method has two starting points, so the second guess has no bearing on the final converged values. The system checks if the postulated

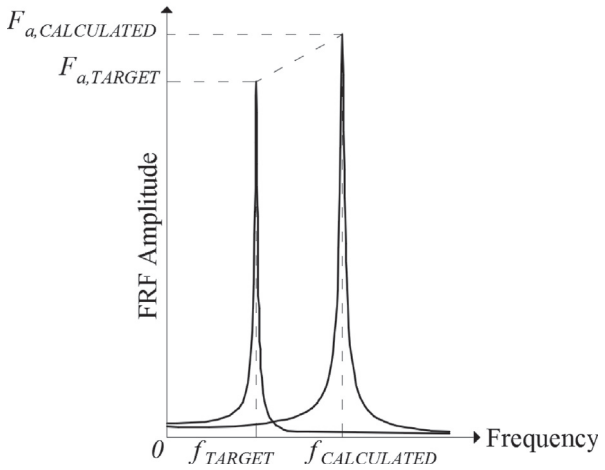

Fig. 5. FRF schematic and parameter definition.

weightings for the initial guess are correct (by checking if the ratio of the peak information between calculated and target FRF data is within the tolerance). If not, the second guess weightings are applied to the soil model, i.e. the calculated mass weighting is multiplied the pile mass and applied to the relevant pile nodes, and the initial stiffness profile is weighted by the calculated stiffness weighting. Using these new weightings, a new FRF is calculated using the previously described method and again compared to the target FRF data. There now exists two estimates of the system properties, iteration$^{(0)}$ and iteration$^{(1)}$. New mass and stiffness weightings for subsequent iterations are calculated using linear projection, which aims to minimise the difference in the peak heights and peak frequency between the calculated and target acceleration FRF data. The system iterates as shown in the flow chart in Fig. 6 until it converges on operating stiffness and mass weightings that allow the reference numerical model to converge on the FRF of the target model. There are a number of inadmissibility checks built into the model also. Due to the nature of the MDOF system, sometimes the linear projection method may produce negative weightings. Should this occur, the linear projection is re-calculated using the j^{th} and $(j\text{-}2)^{th}$, j^{th} and $(j\text{-}3)^{th}$ … j^{th} and $(j\text{-}i)^{th}$ iterations until admissible weightings are produced. Moreover, the method is designed to reset if convergence is not achieved within 15 iterations. This number 15 is arbitrary, and this check is included due to the potential for significant divergence to occur in the model. Since a high value of mass and stiffness may yield the same frequency as low values (due to their inverse relationship with frequency), it is necessary to allow for this potential divergence with this extra criterion.

4. Analysis

The method shown in the flow chart Fig. 6 is programmed in MATLAB and demonstrated in this section. Section 4.1 presents an example of the algorithm as applied on a step-by-step basis to the Target 1 pile FRF data. Section 4.2 presents a study of the method's resilience to finding the unique solutions for multiple runs (since each run will contain random starting estimates). Section 4.3 presents the results of the analysis on the noise-free target models 1–28. Section 4.4 present the results of the method when applied to noisy simulated data (target models 29–34). Finally, Section 4.5 presents the effect of incorrectly specifying the damping ratio in the reference model and its effect on the sensitivity of the converged response.

4.1. Implementation of algorithm

An example of implementing the algorithm is shown herein. The benchmark 'test' data for this example is Target 1 in Table 1, i.e. a 1 m diameter 21 m long steel pile embedded 20 m in a constant loose sand profile (see Section 2.2 for information on derivation of soil stiffness). For this analysis, the target model was created with an artificial mass weighting of 5 times the pile mass distributed to the pile nodes attached to the top quarter of the springs, and a stiffness weighting of 0.75 times the postulated profile for loose sand. The purpose of this example is to show that the algorithm will converge on values close to these weightings by implementing the procedure in Fig. 6 (minimising differences in peak information from target and calculated FRFs and updating weightings using linear projection). As the analysis uses random numbers to start the procedure, various runs yield slightly different results (see Section 4.2 for further elaboration on this). However, all converged runs complete with the FRF amplitude F_a peak and the frequency within 1% of the target data. An example run is shown in Figs. 7 and 8. The example analysis takes 5 iterations to converge. The results of the first four iterations are shown in Fig. 7. Fig. 8 shows the result of the fifth (and final) iteration, and also shows the converged FRF amplitude F_v and FRF amplitude F_d from the calculated model overlain on the target model data. Note, this is done by way of a check and the actual F_v and F_d data are not used in the updating method, as the assumption is that only a modal hammer and an accelerometer are available to

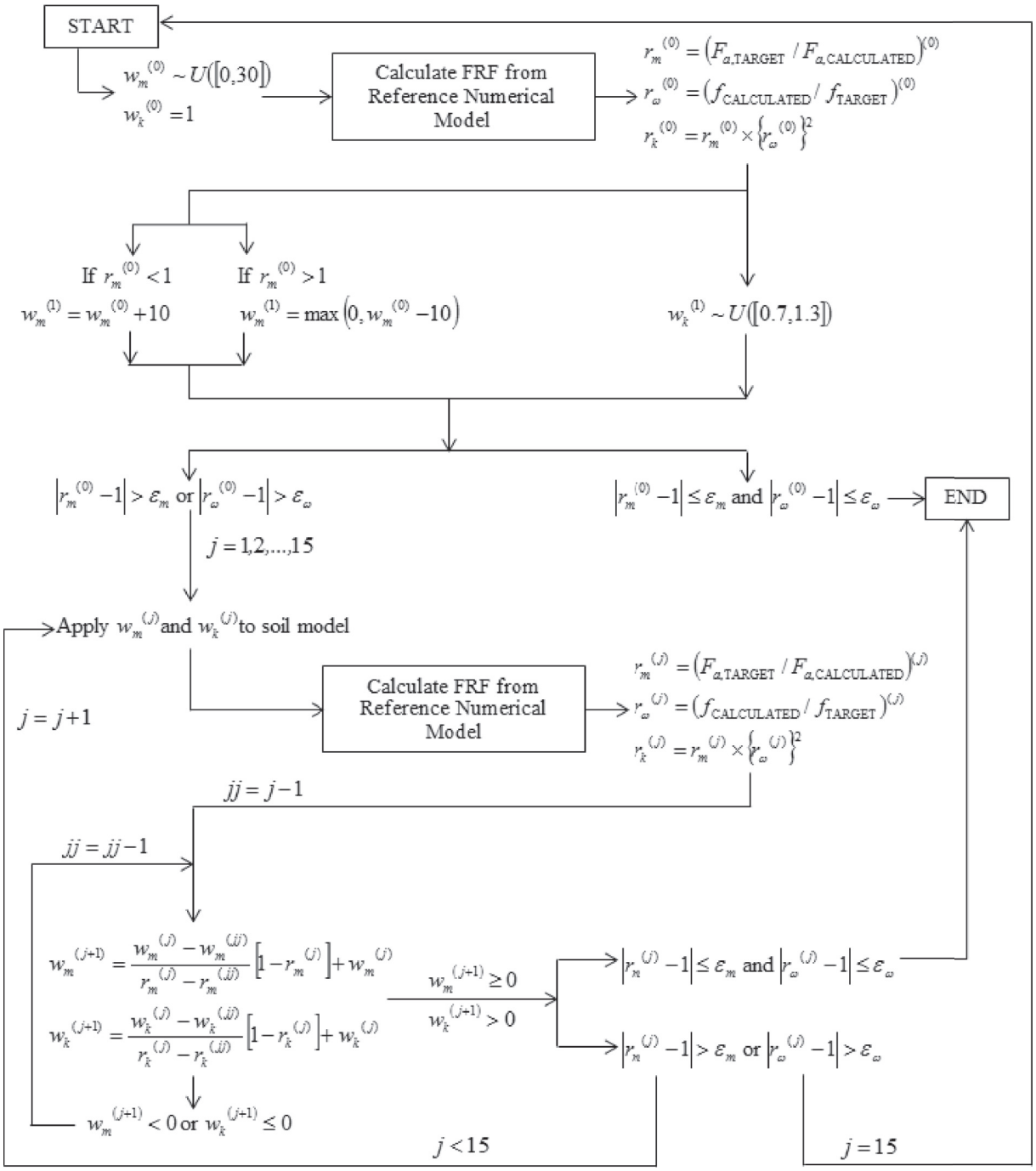

Fig. 6. Flow chart of iterative algorithm.

obtain target data. The stiffness is updated using a combination of the ratio of frequencies and the ratio of F_a peak heights from the acceleration FRF, rather than directly from the ratio of F_d peak heights, however F_d and F_v are produced here to show that the method successfully converges on the correct weightings. Table 2 presents the data for each step of the iteration procedure in more detail. Fig. 7(a) shows the first iteration, obtained by randomly choosing a mass weighting of 27.174 (between 0 and 30) and setting the stiffness weighting to 1. Fig. 7(b) shows the second iteration, where the stiffness weighting is randomly altered to 1.093 (between 0.7 and 1.3, to provide a second guess) and the mass weighting is reduced by 10 to 17.174 (as it was over-predicted in first run – lower peak height in calculated FRF relative to target FRF). Iteration 3 and 4 in Fig. 7(c) and (d) show the implementation of the linear projection algorithm to alter the weightings towards convergence. The mass

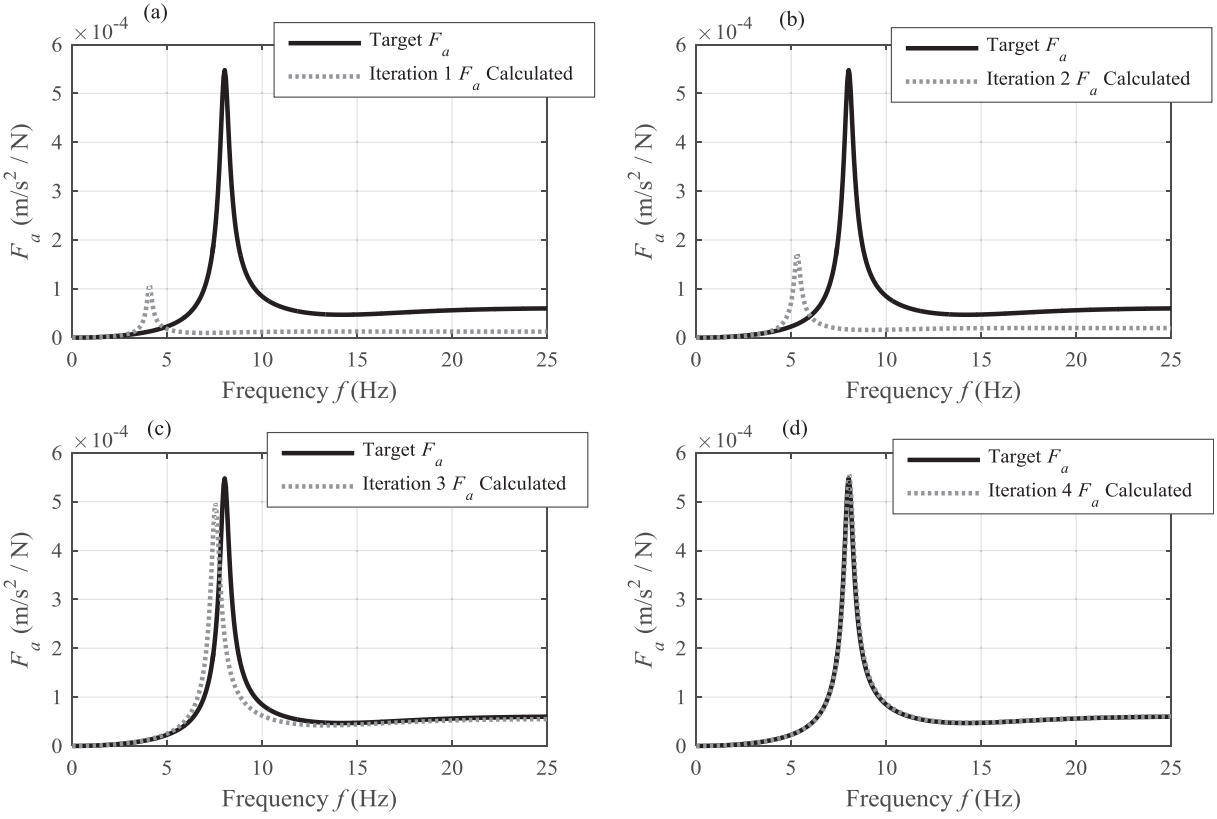

Fig. 7. Iterations in method towards convergence – Target 1 data. (a) Iteration 1, (b) Iteration 2, (c) Iteration 3, (d) Iteration 4.

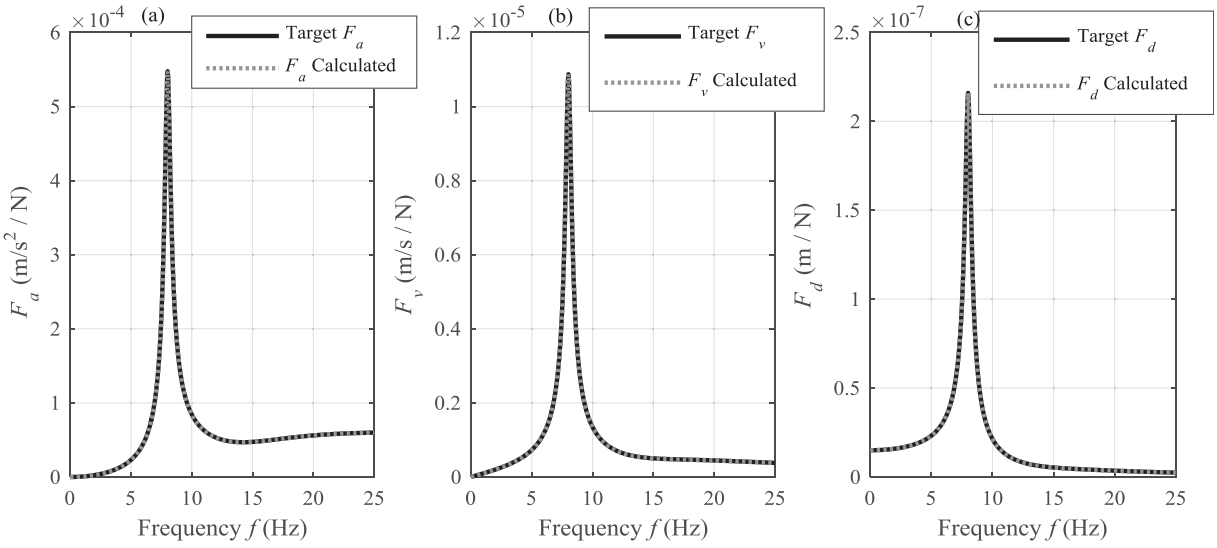

Fig. 8. Converged Frequency Response Functions at iteration 5 (a) F_a, (b) F_v, (c) F_d for Target 1 data.

weighting changes from 5.541 to 4.943, honing in on the target weighting 5, while the stiffness weighting changes from 0.727 to 0.748, tending towards the target value of 0.75. The key point of importance is that the target values are not known to the system, and the method converges using the FRF peak information only.

Fig. 8 shows the converged models (iteration 5), with a converged mass weighting of 4.997 and stiffness weighting of 0.75. Fig. 8(a) shows the converged FRF F_a overlain on the target FRF F_a, Fig. 8(b) shows FRF F_v and Fig. 8(c) shows FRF F_d. Section 4.2

Table 2
Data from iterations for Target 1.

Iteration	w_m Target	w_m Calculated	w_k Target	w_k Calculated	r_m	$\boldsymbol{r}_\omega$	r_k
1	5	27.174	0.75	1	5.032	0.506	1.290
2	5	17.174	0.75	1.093	3.168	0.662	1.390
3	5	5.541	0.75	0.727	1.106	0.940	0.976
4	5	4.943	0.75	0.748	0.990	1.004	0.998
5	5	4.997	0.75	0.750	0.999	1.000	1.000

present the results of multiple runs of the same model to check repeatability and uniqueness of the solution (i.e. that the model does not converge on false matches).

4.2. Model uniqueness with multiple starting estimates

Section 4.1 shows an example of the implementation of the algorithm for one run, in order to highlight the components of the procedure during each iteration. In this section, the results of running the algorithm for ten runs is presented. The model studied herein is the same as previous, i.e. Target 1 data from Table 1. Fig. 9 shows the convergence path for the stiffness and mass weightings (Fig. 9(a) and (b) respectively) and the number of iterations to convergence. Different runs take between 4 iterations and 8 iterations to converge.

Of the ten runs shown in Fig. 9, three converged in 4 iterations, four in 5 iterations and three in 8 iterations. It is noteworthy that the only difference between each run is the random nature in the starting estimates and the resulting effect on the calculated weightings each iteration. Fig. 10 shows the percentage difference between the target mass and stiffness weightings and the converged values for each of the runs shown in Fig. 9. The largest percentage difference in converged mass weighting occurs for Run 7 where the converged mass weighting is 4.977 (Target is 5). By comparison, the largest percentage difference in converged stiffness weighting occurs for Run 4, where the converged value is 0.7486 (Target is 0.75).

4.3. Effect of varying geometrical and material properties

The results of running the algorithm for each of the noise-free target models in Table 1 (Target 1–28) is presented in this section. Table 3 presents the results of a single run of each target model. Each model was run once, and there were no failed trials (each model converged within a reasonable number of iterations). The target mass and stiffness weightings and the converged weightings are shown in each row, as well as the number of iterations required to converge. Note, the number of iterations to converge may change each time the method is run, as this is only really dependent on the random starting estimates in the first two iterations for mass and stiffness weightings. Their inclusion is to highlight that each model converged within the 15 iterations required before resetting of the algorithm. The results in Table 3 highlight that the method

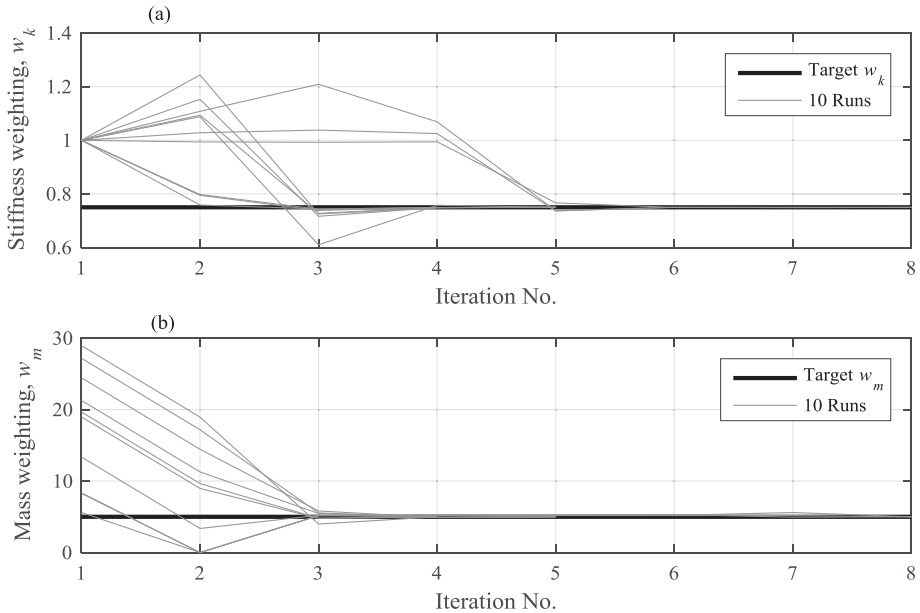

Fig. 9. Convergence of Target 1 data (a) Stiffness weighting, w_k, (b) Mass weighting, w_m.

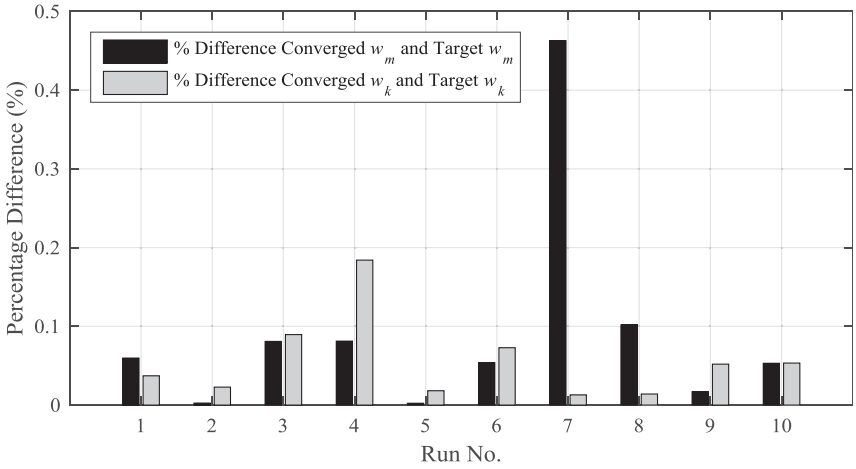

Fig. 10. Target 1 data –Percentage difference in converged w_m and w_k against the target values for 10 runs.

Table 3
Converged results for 28 target models.

Name	Target w_m	Target w_k	Converged w_m	Converged w_k	Iterations
Target 1	5	0.75	4.997	0.750	5
Target 2	5	0.85	5.004	0.850	4
Target 3	5	1.15	5.004	1.150	5
Target 4	5	1.25	4.999	1.251	8
Target 5	10	0.75	9.994	0.750	5
Target 6	10	0.85	9.960	0.849	4
Target 7	10	1.15	9.946	1.1531	4
Target 8	10	1.25	10.003	1.250	5
Target 9	5	0.75	4.981	0.756	4
Target 10	5	0.85	4.997	0.850	5
Target 11	5	1.15	5.004	1.152	5
Target 12	5	1.25	4.990	1.245	4
Target 13	10	0.75	9.999	0.750	6
Target 14	10	0.85	10.098	0.850	3
Target 15	10	1.15	10.044	1.151	5
Target 16	10	1.25	10.015	1.251	5
Target 17	5	0.75	5.004	0.749	5
Target 18	10	1.25	9.963	1.247	3
Target 19	5	0.75	4.965	0.748	3
Target 20	10	1.25	9.939	1.248	4
Target 21	5	0.75	5.012	0.749	4
Target 22	10	1.25	10.043	1.249	3
Target 23	5	0.75	5.001	0.750	7
Target 24	10	1.25	10.001	1.250	4
Target 25	5	0.75	4.985	0.751	5
Target 26	10	1.25	9.961	1.258	4
Target 27	5	0.75	4.998	0.750	4
Target 28	10	1.25	9.973	1.250	7

is insensitive to changes in the geometrical properties of the system, i.e. it is not biased towards flexible piles or otherwise (as observed in Figs. 3 and 4, the difference between a flexible and stiff pile behaviour is in the magnitudes of the FRF peaks only, the trend is similar for each case). Moreover, the effect of soil stiffness profile shape or soil density does not impede the approach. Section 4.4 presents the results of the models including noise intrusion.

4.4. Effect of noise intrusion

The previous analyses were conducted assuming the target data is theoretical perfect, i.e. the results had no errors induced due to noise. In reality, for a pile being tested by impact hammer, there will be some noise intrusion in the results [21,22,39,40]. This noise comes from sources such as environmental influences and sensor resolutions errors. This noise will affect the quality of the signal and introduce errors in the target peak height. In this section, the degree to which added noise

impedes the approach is investigated in terms of the errors in convergence obtained between the target and calculated weighting results. Any errors in the target peak should increase the error in converged weightings.

Six target models (Target 29–34) are created with noise added to the output acceleration signals. During the procedure to develop FRFs, this noise is included. As mentioned, the method from Lyons [48] is used to add noise based on the SNR. Signals with SNRs of 20, 10 and 5 are trialled, for two sets of target mass and stiffness weightings, see Table 1. Note, noise is not added to the hammer signal for this analysis for three main reasons, (i) the method described in Lyons [48] leads to unrealistic noise levels for impulse-type hammer signals due to the high signal variance, (ii) real impulse tests have shown that noise intrusion in modal hammers is typically quite low [22], and (iii) since it is assumed that once the hammer ceases contact with the pile post-impulse, no further contact is made and thus this input to the updating algorithm can be automatically set to zero, to allow free vibration.

To visualise the effect of noise, Fig. 11 shows the simulated acceleration signal and FRF for a model pile with zero noise and with SNR = 20, 10 and 5. Target models 1, 29, 31 and 33 are compared (same geometric properties and target weightings – see Table 1) in this plot. Fig. 11(a) shows the acceleration signals for no noise and three different noise levels. Fig. 11(b) shows the FRF amplitude of each signal. As is evident, the effect of noise is to add random oscillations to the peak FRF amplitude. The effect of these errors on the accuracy of the approach is investigated below.

Target models 29–34 (with varying amounts of added noise) are analysed herein. Each model is run once and the converged values for mass and stiffness weighting are shown in Table 4. Fig. 12 shows the converged FRF amplitude plots for Target model 34, for F_a, F_v and F_d, when the target model had a high SNR of 5. As can be seen, the model successfully converges even in the case of high noise intrusion.

Table 4 shows the converged results for one run of each of the Target models 29–34 (see Table 1 for properties). The converged mass and stiffness weightings deviate a little more from the target values than in the noise free cases in Table 3. The maximum percentage difference in all cases run in Table 3 was 0.97% for converged mass weighting and 0.76% for converged stiffness weighting. This compares with a maximum percentage difference of 4.3% for converged mass weighting and 4.17% for converged stiffness weighting for the added noise cases. The maxima in both the latter cases occurred for the Target 34 data with SNR = 5, so is not unexpected as this had the highest noise pollution. Broadly speaking, however, all models converge on close to the correct values (i.e. there are no false convergences on weightings away from the target). Section 4.5 investigates the effect of incorrect damping on the convergence.

4.5. Effect of discrepancies in damping ratio

The analyses presented so far have assumed that the damping ratio is known from the target models, i.e. it would have been accurately measured from the 'impact test data' using an approach such as logarithmic decrement technique or otherwise, applied to the response signals. In reality, there may be some error in the accurate measurement of this parameter. While not unreasonable to assume the geometrical and material properties of a pile would be known to the user for the purpose of creating the reference model, properties such as damping may be more error-prone. In this section, a brief analysis is conducted to assess the impact of an incorrectly specified damping ratio on the success of the iterative approach. The data

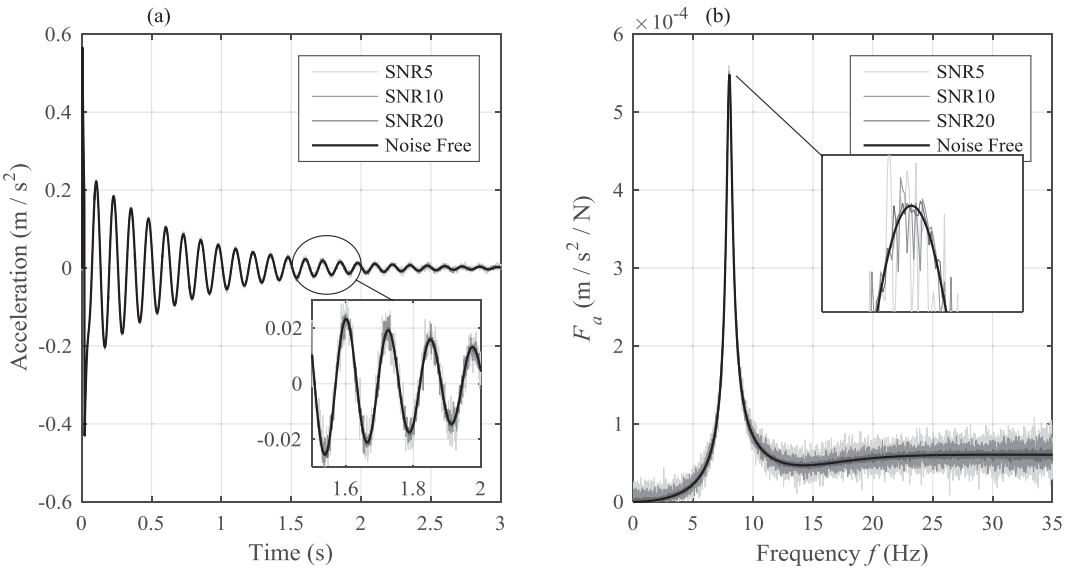

Fig. 11. Effect of added noise on FRF peak, (a) Acceleration signals due to impulse – no noise, SNR = 20, SNR = 10 and SNR = 5 [Inset] zoomed in between $t = 1.5$s and $t = 2$s, (b) FRF amplitude of acceleration with various noise levels [Inset] effect of noise on peak FRF amplitude.

Table 4
Convergence results for models with added noise.

Name	Target w_m	Target w_k	Converged w_m	Converged w_k	SNR	Iterations
Target 29	5	0.75	4.975	0.744	20	4
Target 30	10	1.25	10.002	1.248	20	4
Target 31	5	0.75	4.900	0.732	10	4
Target 32	10	1.25	9.793	1.228	10	4
Target 33	5	0.75	4.859	0.733	5	5
Target 34	10	1.25	9.577	1.199	5	4

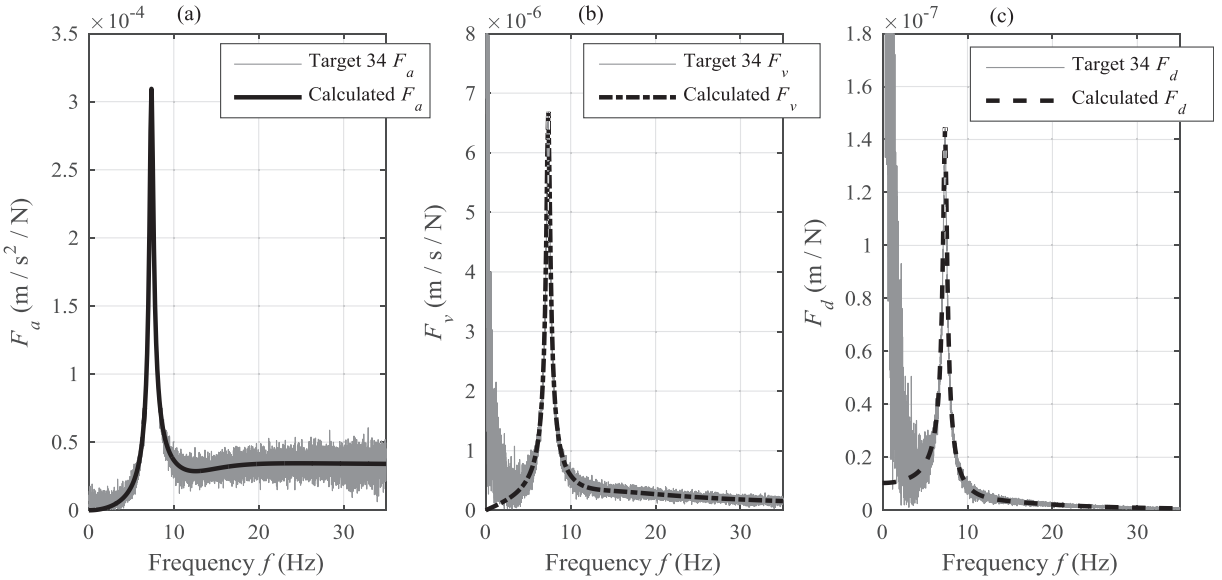

Fig. 12. Converged Target 34 analysis – SNR = 5. (a) F_a, (b) F_v, (c) F_d.

from Target 1 is used, and the 3% damping ratio (mode 1) used in Target 1 is varied by (i) ±10% to $\xi_1 = 2.7\%$ and $\xi_1 = 3.3\%$, respectively, (ii) ±20% to $\xi_1 = 2.4\%$ and $\xi_1 = 3.6\%$, respectively and (iii) ±30% to $\xi_1 = 2.1\%$ and $\xi_1 = 3.9\%$, respectively, for the generated reference models used in the model updating procedure. For each erroneous damping ratio, the method is run 10 times. The results are shown in Table 5.

The results in Table 5 show that running the iterative procedure for the Target 1 data with incorrectly specified damping ratio for the first mode leads to a moderately nonlinear change in the average percentage difference for different amounts of damping error. Under- and overestimating the damping ratio by 10% leads to an average percentage difference of the order of −12% and +11% respectively between both the target and calculated mass and stiffness weightings. A difference of ±20% leads to an average percentage difference of approximately −26% and +22% between both target and calculated weightings. Finally, a difference in damping ratio of ±30% leads to an average percentage difference of approximately −41% and +31% between target and calculated weightings. This brief analysis highlights the importance of an accurate specification of damping ratio in the reference model, to ensure accurate weightings are obtained. Underestimating damping leads to a higher error for this data set than overestimating damping. Of note is that the error in mass and stiffness weighting is approximately the same in each case because the corresponding modal frequency is assumed to be accurate.

Table 5
Results of varying damping ratio in reference model.

Analysis	ξ_{Target}	$\xi_{\text{Specified}}$	% Difference Average±Standard Deviation w_m	% Difference Average±Standard Deviation w_k
Underestimate Target ξ by 10%	0.03	0.027	−12.41 ± 0.14	−12.50 ± 0.37
Overestimate Target ξ by 10%	0.03	0.033	+11.44 ± 0.18	+11.2 ± 0.05
Underestimate Target ξ by 20%	0.03	0.024	−26.03 ± 0.35	−26.17 ± 0.26
Overestimate Target ξ by 20%	0.03	0.036	+21.97 ± 0.42	+21.5 ± 0.08
Underestimate Target ξ by 30%	0.03	0.021	−41.1 ± 0.33	−41.32 ± 0.36
Overestimate Target ξ by 30%	0.03	0.039	+31.68 ± 0.49	+30.85 ± 0.22

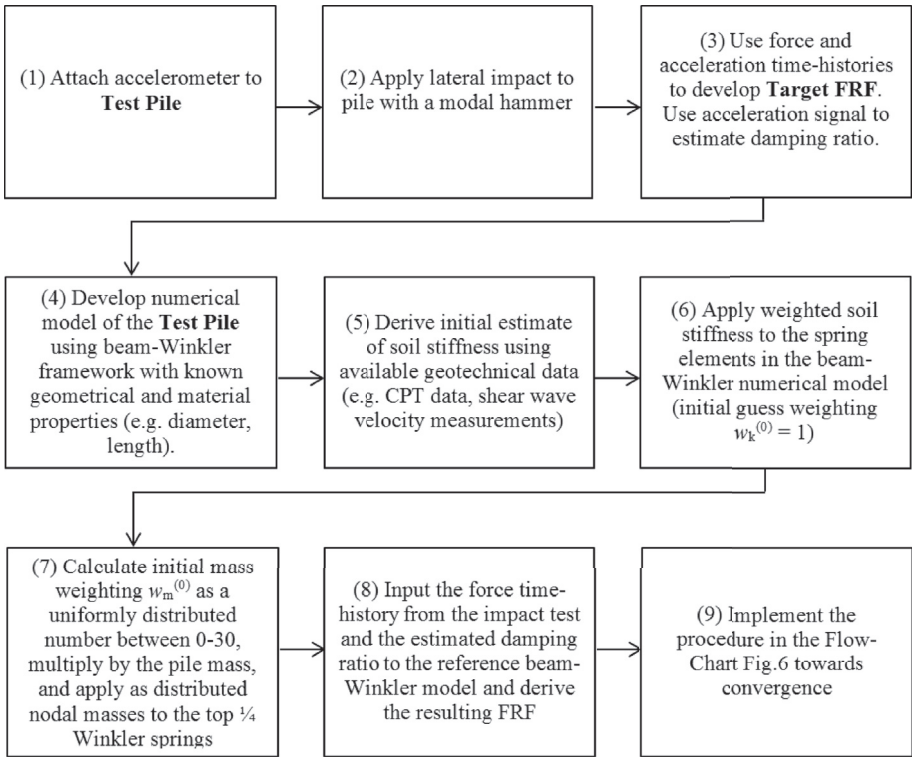

Fig. 13. Procedure for application to real pile structures.

5. Procedure for application of method to real piles

The previous sections introduced the FE updating approach as applied to numerically simulated target data. In this section, a summary of the procedure for application to real piles is presented. Fig. 13 presents a flow-chart of the procedure to apply the method to a real pile to estimate the operating soil stiffness and mass profiles on the real system. For step (3), the damping ratio can be estimated from the acceleration time-history using approaches such as the logarithmic decrement technique [52] or by fitting exponential curves [53] among other approaches. For step (5), representative soil stiffness can be derived from geotechnical data using a variety of approaches, see examples [11,21,22,54]. Using available geotechnical data such as shear wave velocity measurements or CPT data close to the test pile can provide an indication of the shape of the soil stiffness profile with depth, which can subsequently be adjusted by the weighting factors in the algorithm. Note, Fig. 13 is not an exhaustive guide for application of the approach to real piles, its purpose is to summarise the main steps. Fig. 13 is best read in conjunction with Fig. 6, which details the individual steps in the updating algorithm.

6. Conclusion

In this paper, an iterative approach to obtain operating soil mass and stiffness profiles in dynamic beam-Winkler models is presented. The method aims to address the significant uncertainty present in the operational characteristics of soil-pile systems, and the growing importance of the accurate characterisation of soil-structure interface stiffness for offshore wind and SHM applications, among others.

The iterative method is based on FRF data, and uses differences in FRF peaks and frequencies between calculated and target models to converge on soil mass and stiffness weightings. The approach is demonstrated using numerically simulated data in this paper, through the generation of target models. Target data representing a range of pile geometries, soil densities, and stiffness distributions are created to test the procedure. The model is successfully applied to a range of target cases, with varying geometrical properties and operating soil mass and stiffness. In all cases, the method converges on correct weightings and is unaffected by soil density changes or the shape of the soil profile (assuming the shape is known beforehand, i.e. from site investigation data or otherwise). The effect of noise on the approach is investigated, and although the errors in the converged weightings do increase, the method still converges in the correct region even for high noise pollution, i.e. the solution is unique and there are no false convergences. Finally, the effect of incorrectly specifying the damping ratio in the generated reference model is checked. The errors in converged weightings vary somewhat nonlinearly with the error in damping, however the magnitude of the error is approximately the same for both the converged mass and stiffness weighting

in each case. This study highlights the importance of accurate specification of damping for the successful application of the method.

The FRF-based model updating method was demonstrated using simulated numerical data in this paper. This was undertaken as it was possible to observe exactly if the method converged on the correct weightings. It should be noted that there is potential for some errors with the application of the approach to real piles, in that a numerical reference model of a pile will deviate in behaviour somewhat from a real pile embedded in soil. Moreover, the method relies on the user knowing the geometrical and material properties of a given test pile, which may also be a source of some uncertainty. Engineering judgement may be required in the event of a false convergence in the real case. A false convergence may be understood to occur if the method converges on a very stiff or weak stiffness profile where the geotechnical data indicated otherwise. Future work will expand the approach developed in this paper to experimental pile data with a view to understanding these potential issues.

Acknowledgements

This research was enabled through funding obtained from the Royal Irish Academy Charlemont Scholarship Research Travel Awards 2016. One of the authors is funded by the EU H2020 project SAFE-10-T (Project No. 723254).

References

[1] A.E. Kampitsis, E.J. Sapountzakis, S.K. Giannakos, N. a. Gerolymos, Seismic soil–pile–structure kinematic and inertial interaction—a new beam approach, Soil Dynam. Earthq. Eng. 55 (2013) 211–224, https://doi.org/10.1016/j.soildyn.2013.09.023.
[2] R.W. Boulanger, C.J. Curras, B.L. Kutter, D.W. Wilson, A. Abghari, Seismic soil-pile-structure interaction experiments and analysis, J. Geotech. Geoenviron. Eng. 125 (1999) 750–759.
[3] L.J. Prendergast, K. Gavin, P. Doherty, An investigation into the effect of scour on the natural frequency of an offshore wind turbine, Ocean Eng. 101 (2015) 1–11, https://doi.org/10.1016/j.oceaneng.2015.04.017.
[4] W.G. Versteijlen, A.V. Metrikine, K.N. van Dalen, A method for identification of an effective Winkler foundation for large-diameter offshore wind turbine support structures based on in-situ measured small-strain soil response and 3D modelling, Eng. Struct. 124 (2016) 221–236, https://doi.org/10.1016/j.engstruct.2016.06.007.
[5] S. Foti, D. Sabia, Influence of foundation scour on the dynamic response of an existing bridge, J. Bridge Eng. 16 (2011) 295–304, https://doi.org/10.1061/(ASCE)BE.1943-5592.0000146.
[6] L.J. Prendergast, D. Hester, K. Gavin, Determining the presence of scour around bridge foundations using vehicle-induced vibrations, J. Bridge Eng. 21 (2016), https://doi.org/10.1061/(ASCE)BE.1943-5592.0000931.
[7] T. Bao, R. Andrew Swartz, S. Vitton, Y. Sun, C. Zhang, Z. Liu, Critical insights for advanced bridge scour detection using the natural frequency, J. Sound Vib. 386 (2017) 116–133, https://doi.org/10.1016/j.jsv.2016.06.039.
[8] C.-C. Chen, W.-H. Wu, F. Shih, S.-W. Wang, Scour evaluation for foundation of a cable-stayed bridge based on ambient vibration measurements of superstructure, NDT E Int. 66 (2014) 16–27, https://doi.org/10.1016/j.ndteint.2014.04.005.
[9] B. Byrne, R. McAdam, H. Burd, G. Houlsby, C. Martin, L. Zdravković, D. Taborda, D. Potts, R. Jardine, M. Sideri, F. Schroeder, K. Gavin, P. Doherty, D. Igoe, A. Muir Wood, D. Kallehave, J. Skov Gretlund, New design methods for large diameter piles under lateral loading for offshore wind applications, in: Int. Symp. Front. Offshore Geotech., Oslo, 2015, pp. 705–710. https://www.researchgate.net/profile/Byron_Byrne/publication/280620361_New_design_methods_for_large_diameter_piles_under_lateral_loading_for_offshore_wind_applications/links/55bf28fb08aed621de121f29.pdf. (Accessed 20 April 2017).
[10] L. Arany, S. Bhattacharya, J. Macdonald, S.J. Hogan, Design of monopiles for offshore wind turbines in 10 steps, Soil Dynam. Earthq. Eng. 92 (2017) 126–152, https://doi.org/10.1016/j.soildyn.2016.09.024.
[11] API, API RP2A-WSD, 2007.
[12] J.M. Murchison, M.W. O'Neill, Evaluation of p-y relationships in cohesionless soils, in: Anal. Des. Pile Found. Proc. A Symp. Conjunction with ASCE Natl. Conv, 1984, pp. 174–191.
[13] S.K. Suryasentana, B.M. Lehane, Numerical Derivation of CPT-based P – Y Curves for Piles in Sand, Geotechnique, 2013.
[14] E.P. Carden, P. Fanning, Vibration based condition monitoring: a review, Struct. Health Monit. 3 (2004) 355–377, https://doi.org/10.1177/1475921704047500.
[15] W. Fan, P. Qiao, Vibration-based damage identification methods: a review and comparative study, Struct. Health Monit. 10 (2010) 83–111, https://doi.org/10.1177/1475921710365419.
[16] L.J. Prendergast, K. Gavin, D. Hester, Isolating the location of scour-induced stiffness loss in bridges using local modal behaviour, J. Civ. Struct. Heal. Monit. (2017), https://doi.org/10.1007/s13349-017-0238-3.
[17] W. Xiong, C.S. Cai, B. Kong, P. Tang, J. Ye, Identification of bridge scour depth by tracing dynamic behaviors of superstructures, KSCE J. Civ. Eng. (2017) 1–12, https://doi.org/10.1007/s12205-017-1409-9.
[18] S.H. Ju, Determination of scoured bridge natural frequencies with soil–structure interaction, Soil Dynam. Earthq. Eng. 55 (2013) 247–254, https://doi.org/10.1016/j.soildyn.2013.09.015.
[19] L.J. Prendergast, D. Hester, K. Gavin, Development of a vehicle-bridge-soil dynamic interaction model for scour damage modelling, Shock Vib. 2016 (2016).
[20] J.L. Briaud, S. Hurlebaus, K. Chang, C. Yao, H. Sharma, O. Yu, C. Darby, B.E. Hunt, G.R. Price, Realtime Monitoring of Bridge Scour Using Remote Monitoring Technology, 2011. Austin, TX, http://tti.tamu.edu/documents/0-6060-1.pdf.
[21] L.J. Prendergast, D. Hester, K. Gavin, J.J. O'Sullivan, An investigation of the changes in the natural frequency of a pile affected by scour, J. Sound Vib. 332 (2013) 6685–6702. https://doi.org/10.1016/j.jsv.2013.08.020i.
[22] L.J. Prendergast, K. Gavin, A comparison of initial stiffness formulations for small-strain soil – pile dynamic Winkler modelling, Soil Dynam. Earthq. Eng. 81 (2016) 27–41, https://doi.org/10.1016/j.soildyn.2015.11.006.
[23] J. Sadrekarimi, M. Akbarzad, Comparative study of methods of determination of coefficient of subgrade reaction, Electron. J. Geotech. Eng. 14 (2009).
[24] M. Imregun, W.J. Visser, Ewins, finite element model updating using frequency response function Data—I. Theory and initial investigation, Mech. Syst. Signal Process. 9 (1995) 187–202, https://doi.org/10.1006/mssp.1995.0015.
[25] N. Nalitolela, J.E.T. Penny, M.I. Friswell, Updating model parameters by adding an imagined stiffness to the structure, Mech. Syst. Signal Process. 7 (1993) 161–172, https://doi.org/10.1006/mssp.1993.1005.
[26] J.E. Mottershead, M. Link, M.I. Friswell, The sensitivity method in finite element model updating: a tutorial, Mech. Syst. Signal Process. 25 (2011) 2275–2296, https://doi.org/10.1016/j.ymssp.2010.10.012.
[27] H.Y. Hwang, C. Kim, Damage detection in structures using a few frequency response measurements, J. Sound Vib. 270 (2004) 1–14, https://doi.org/10.1016/S0022-460X(03)00190-1.

[28] A. Esfandiari, F. Bakhtiari-Nejad, A. Rahai, M. Sanayei, Structural model updating using frequency response function and quasi-linear sensitivity equation, J. Sound Vib. 326 (2009) 557–573, https://doi.org/10.1016/j.jsv.2009.07.001.
[29] J.E. Mottershead, M.I. Friswell, Model updating in structural dynamics: a survey, J. Sound Vib. 167 (1993) 347–375, https://doi.org/10.1006/jsvi.1993.1340.
[30] R.M. Lin, D.J. Ewins, Analytical model improvement using frequency response functions, Mech. Syst. Signal Process. 8 (1994) 437–458, https://doi.org/10.1006/mssp.1994.1032.
[31] R.M. Lin, J. Zhu, Model updating of damped structures using FRF data, Mech. Syst. Signal Process. 20 (2006) 2200–2218, https://doi.org/10.1016/j.ymssp.2006.05.008.
[32] H.G. Natke, Updating computational models in frequency domain based on measured data: a survey, Probabilist. Eng. Mech. 3 (1988) 28–35, https://doi.org/10.1016/0266-8920(88)90005-7.
[33] Y.W. Kwon, H. Bang, The Finite Element Method Using MATLAB, CRC Press, Inc., Boca Raton, FL, 2000.
[34] E. Winkler, Theory of Elasticity and Strength, Dominicus Prague, 1867.
[35] S.C. Dutta, R. Roy, A critical review on idealization and modeling for interaction among soil–foundation–structure system, Comput. Struct. 80 (2002) 1579–1594, https://doi.org/10.1016/S0045-7949(02)00115-3.
[36] R.W. Clough, J. Penzien, Dynamics of Structures, 1993.
[37] J.W. Tedesco, W.G. McDougal, C. Allen Ross, Structural Dynamics: Theory and Applications, 1999.
[38] R.V. Dukkipati, Matlab for Mechanical Engineers, New Age Science, 2009.
[39] F. Dezi, F. Gara, D. Roia, Dynamic response of a near-shore pile to lateral impact load, Soil Dynam. Earthq. Eng. 40 (2012) 34–47, https://doi.org/10.1016/j.soildyn.2012.04.002.
[40] F. Dezi, F. Gara, D. Roia, Experimental study of near-shore pile-to-pile interaction, Soil Dynam. Earthq. Eng. 48 (2013) 282–293, https://doi.org/10.1016/j.soildyn.2013.01.025.
[41] S. Donohue, M. Long, K. Gavin, P. O'Connor, Shear wave stiffness of Irish glacial till, in: Int. Conf. Site Characterisation I, Porto, Portugal, 2004, pp. 459–466.
[42] R.J. Jardine, F.C. Chow, R.F. Overy, J. Standing, ICP Design Methods for Driven Piles in Sands and Clays, 2005. London.
[43] S.A. Ashford, T. Juirnarongrit, Evaluation of pile diameter effect on initial modulus of subgrade reaction, Geotech. Geoenviron. Eng. 129 (2003) 234–242, https://doi.org/10.1061/(ASCE)1090-0241(2003)129:3(234).
[44] R.P.2A. API, Recommended Practice for Planning, Designing and Constructing Offshore Platforms - Working Stress Design, 2007. Washington, DC.
[45] T. Lunne, H.P. Christopherson, Interpretation of Cone penetrometer data for offshore sands, in: Offshore Technol. Conf. OTC4464, Houston, Texas, 1983.
[46] T. Lunne, P.K. Robertson, J.J.M. Powell, Cone Penetration Testing in Geotechnical Practice, Blackie Academic and Professional, 1997.
[47] F. Schnaid, B.M. Lehane, M. Fahey, In situ test characterisation of unusual geomaterials, in: Proc. Int. Conf. Site Characterisation, Porto, Portugal, 2004, pp. 49–73.
[48] R. Lyons, Understanding Digital Signal Processing, third ed., Prentice Hall, Boston, MA, 2011.
[49] Fugro, Guide for Estimating Soil Type and Characteristics Using Cone Penetration Testing, Cone Penetration Tests, 2011. http://www.fes.co.uk/downloads/CPT-general.pdf. (Accessed 12 May 2014).
[50] L.J. Prendergast, C. Reale, K. Gavin, Probabilistic examination of the change in eigenfrequencies of an offshore wind turbine under progressive scour incorporating soil spatial variability, Mar. Struct. 57 (2018) 87–104, https://doi.org/10.1016/j.marstruc.2017.09.009.
[51] L.J. Prendergast, K. Gavin, Chapter 15 - monitoring of scour critical bridges using changes in the natural frequency of vibration of foundation piles: a preliminary investigation, Mater. Infrastruct. 1 (2016) 199–209.
[52] A.K. Chopra, Dynamics of Structures. A Primer, Earthquake Engineering Research Institute, 1981.
[53] G. Gutenbrunner, K. Savov, H. Wenzel, Sensitivity studies on damping estimation, in: Proc. Second Int. Conf. Exp. Vib. Anal. Civ. Eng. Struct., Porto, Portugal, 2007. http://www.vce.at/pdf/downloads/Publications/Damping Estimation.pdf. (Accessed 9 March 2012).
[54] S. Li, S. He, H. Li, Y. Jin, Scour depth determination of bridge piers based on time-varying modal parameters: application to Hangzhou Bay bridge, J. Bridge Eng. 22 (2017), https://doi.org/10.1061/(ASCE)BE.1943-5592.0001154.